

THE OFFICIAL MAGAZINE OF THE OCEANOGRAPHY SOCIETY

Oceanography

CITATION

Sgroi, T., S. Monna, D. Embriaco, G. Giovanetti, G. Marinaro, and P. Favali. 2014. Geohazards in the Western Ionian Sea: Insights from non-earthquake signals recorded by the NEMO-SN1 seafloor observatory. *Oceanography* 27(2):154–166, <http://dx.doi.org/10.5670/oceanog.2014.51>.

DOI

<http://dx.doi.org/10.5670/oceanog.2014.51>

COPYRIGHT

This article has been published in *Oceanography*, Volume 27, Number 2, a quarterly journal of The Oceanography Society. Copyright 2014 by The Oceanography Society. All rights reserved.

USAGE

Permission is granted to copy this article for use in teaching and research. Republication, systematic reproduction, or collective redistribution of any portion of this article by photocopy machine, reposting, or other means is permitted only with the approval of The Oceanography Society. Send all correspondence to: info@tos.org or The Oceanography Society, PO Box 1931, Rockville, MD 20849-1931, USA.

Geohazards in the Western Ionian Sea

Insights from Non-Earthquake Signals Recorded
by the NEMO-SN1 Seafloor Observatory

BY TIZIANA SGROI, STEPHEN MONNA, DAVIDE EMBRIACO,
GABRIELE GIOVANETTI, GIUDITTA MARINARO, AND PAOLO FAVALI



ABSTRACT. Seafloor instability resulting from both tectonics and volcanism affects the Western Ionian Sea. The NEutrino Mediterranean Observatory-Submarine Network 1 (NEMO-SN1), deployed 25 km offshore eastern Sicily at 2,100 m water depth, records a variety of signals for geophysical and environmental long-term monitoring, including non-earthquake seismic signals that provide insights into the area's geohazards. The signals analyzed for this paper are: (1) seismic signals associated with submarine landslides, (2) volcanic tremor, and (3) short duration events (SDEs). These seismic signals are analyzed together with pressure and hydrophone data to help identify their origins. Tectonic shifts can lead to submarine landslides. Volcanic tremor is the result of sustained pressure fluctuations, probably related to stress variations induced by magma movement. Increased tremor amplitudes recorded at NEMO-SN1 during lava fountain episodes from February to April 2013 suggest the presence of an east-southeast offshore location of the roots of Mt. Etna's magma feeding system. SDEs are thought to result from hydrofracturing of carbonate outcroppings at the base of the Malta Escarpment that is possibly induced by changes in the stress field associated with magma movement.

INTRODUCTION

At present, there is an effort to install permanent underwater monitoring infrastructure at a global scale (Favali et al., 2010). In the western Ionian Sea (off eastern Sicily), the NEutrino Mediterranean Observatory-Submarine Network 1 (NEMO-SN1), a cabled node of the EMSO infrastructure (European Multidisciplinary Seafloor and water-column Observatory, <http://www.emso-eu.org>; see sidebar on page 167) is operating in real time in water depths of about 2,100 m (Favali et al., 2013). This site was chosen for its high seismic and volcanic hazard, which is related to its proximity to seismogenic structures and to Mt. Etna. The study area is part of the complex geodynamics of the Central Mediterranean region, which is driven mainly by convergence of the European and African Plates and by gravitational sinking and rollback of oceanic lithosphere (Argnani, 2009, and references therein). In the offshore area, the Malta Escarpment (Figure 1) is a regional fault

system more than 150 km long, mostly submerged, and trending NNW-SSE that separates the subduction zone's foreland basin from the oceanic crust beneath the Ionian Sea (Scandone et al., 1981; Ben-Avraham et al., 1995; Hirn et al., 1997; Bianca et al., 1999; Meletti et al., 2000). These seismogenic structures have caused the most destructive earthquakes in Italy (e.g., M6.6 in 1169, M7.4 in 1693, M7.2 in 1908; Boschi et al., 2000), and they have also generated strong tsunamis (Tinti et al., 2004). The same structures are also considered possible sources of significant microseismicity, which is not properly detected by the land network (Sgroi et al., 2007).

Within the geological context of the Calabrian Arc subduction system, Mt. Etna rises to 3,350 m and is one of the world's largest and most active basaltic volcanoes. Its eastern flank extends beneath the sea surface to 2,000 m depth. Mt. Etna has been nearly persistently active for the last 600,000 years (Branca et al., 2011). At present, its activity is

mostly localized in the higher part of the volcanic edifice. Another possible source of hazard in the area comes from the interplay between regional tectonic activity along the Malta Escarpment and gravitational instability of the Mt. Etna volcanic edifice (McGuire, 1996). Some researchers link Mt. Etna activity to large extensional faults located offshore because the basal portion of its eastern flank is located at sea and is intersected by the Malta Escarpment (Borgia et al., 1992, 2000; McGuire, 1996; Hirn et al., 1997). Eastward movement of the volcanic edifice over a stationary magma supply may be the cause of an apparent westward migration of volcanic activity (Borgia et al., 1992).

Volcanic and tectonic structures are known seismic signal sources. Additional sources are tidal variations and currents that affect the stress state of the western Ionian seafloor. Seabed disturbance occurs as a result of bottom shear stress, the combined force that waves and currents exert on the seafloor (Dalyander et al., 2013). Here, we focus on three types of non-earthquake seismic signals: (1) submarine landslides, (2) volcanic tremor, and (3) short duration events (SDEs). The main objective of this paper is to show how these signals are related to the known hazards of the western Ionian Sea and how continuous, real-time recording of these signals could have a significant impact on hazard assessment. This multidisciplinary study is mostly based on real-time data collected by the cabled NEMO-SN1 seafloor observatory during the period September 2012 to May 2013 and on data collected during the 2002–2003 stand-alone NEMO-SN1 campaign (Favali et al., 2013).

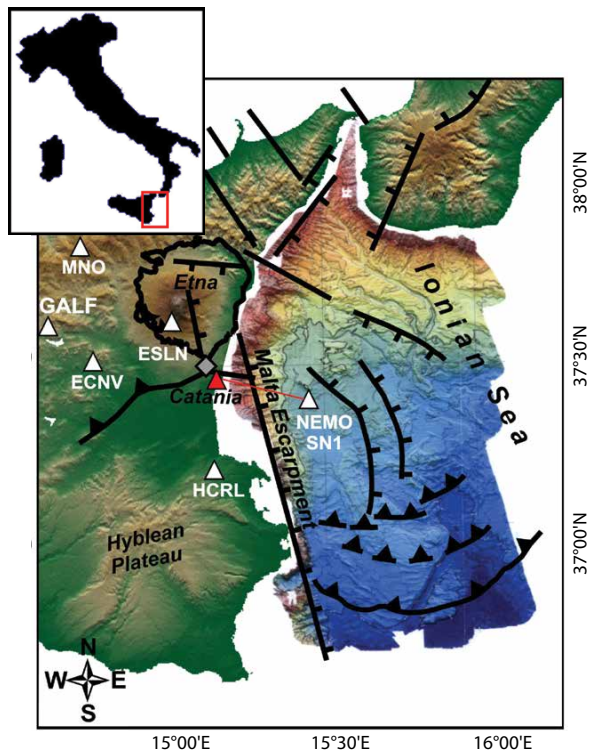


Figure 1. Western Ionian Sea multibeam map (Marani et al., 2004). The inset shows the location of the study area in Southern Italy. The white triangles indicate the location of the NEutrino Mediterranean Observatory-Submarine Network 1 (NEMO-SN1) seafloor observatory and of the land stations used for comparison (ESLN, ECVN, GALF, MNO, HCRL). The red triangle shows the onshore laboratory in Catania's harbor. Geological structures (from Meletti et al., 2000; Marani et al., 2004; Argnani and Bonazzi, 2005) are also shown: continuous lines refer to strike-slip faults, lines with ticks represent extensional faults, and lines with black triangles are thrusts and reverse faults.

THE NEMO-SN1 SEAFLOOR OBSERVATORY

The NEMO-SN1 cabled seafloor observatory is equipped with many geophysical and oceanographic sensors (Favali et al., 2013). All of the data collected by the instruments are transferred in real time to the onshore laboratory located at the Laboratori Nazionali del Sud-Istituto Nazionale di Fisica Nucleare at Catania's harbor. A 28 km long electro-optical cable from the shore laboratory to NEMO-SN1 provides power and bi-directional real-time communication for the whole observatory (Figure 1). Users can check real-time diagnostic

information on the whole system and send commands to the observatory control system as well as to each device. It is also possible to reconfigure the observatory mission by switching each instrument on and off and to change the sampling frequencies and other parameters of the different devices.

A common time reference for the various time series, provided by a GPS receiver located at the onshore laboratory, allows us to correlate data from different instruments. The GPS signal is distributed by commercial telemetry hardware (with its proprietary data transfer protocol) over optical fiber to the offshore instruments that operate at higher frequencies (i.e., broadband seismometer, digital hydrophone) so that data are time-stamped at the source. A value of less than 400 ms has been measured for the timing delay due to the transfer of the GPS signal from land to the seafloor. The overall standard deviation of the drift between the GPS clock and the internal seismometer clock is 61 ms, with null average. These errors

are well below the accuracy needed for the present analysis. For lower frequency instruments, time-stamping with the same reference is performed onshore by a local Network Time Protocol (NTP) server synchronized with the GPS receiver. Because the onshore laboratory is linked to the Internet, the whole system is fully remotely operable.

Data from the sensors are permanently archived and published on the Internet (http://www.moist.it/sites/western_ionian_sea/2/SMO1). They are also available in real time for automatic analysis, which is essential for earthquake and tsunami early warning applications. In fact, the NEMO-SN1 seismometer is part of the Italian Seismic Network managed by the Istituto Nazionale di Geofisica e Vulcanologia (INGV). Moreover, seismic and pressure data are analyzed at the onshore station with real-time processes. A dedicated tsunami detection algorithm analyzes pressure data in order to detect anomalous waves that indicate a possible tsunami. The seismometer data acquisition software can detect seismic events by applying an STA/LTA (short time average/long time average) threshold procedure (Chierici et al., 2012). In the case of an alert, the software installed at the shore station sends automatic emails and text messages. An automatic alarm is also sent if a malfunction is detected at any level of the acquisition chain, from the underwater system to the onshore station. In this pilot experiment, alerts are sent to researchers and system managers. In the near future, when all procedures are validated, the alerts will be sent directly to civil protection agencies.

In this paper, we analyze data from three instruments hosted by NEMO-SN1—a broadband seismometer deployed on the seafloor, an absolute

Tiziana Sgroi (tiziana.sgroi@ingv.it) is Research Scientist, Istituto Nazionale di Geofisica e Vulcanologia (INGV), Rome, Italy. **Stephen Monna** is Research Scientist, INGV, Rome, Italy. **Davide Embriaco** is Research Scientist, INGV, Portovenere, Italy. **Gabriele Giovanetti** is Technologist, **Giuditta Marinaro** is Technologist, and **Paolo Favali** is Research Director, all at INGV, Rome, Italy.

pressure gauge, and a hydrophone fixed to the observatory frame. The seismometer is a three-component broadband instrument (Guralp CMG-1T, 0.0027 Hz to 50 Hz bandwidth and 100 Hz sampling rate). The quality of the NEMO-SN1 seismic recordings is high, with a good signal/noise ratio (particularly for frequencies above 1 Hz), mainly a result of site depth and good coupling of the seismometer to the seafloor (Monna et al., 2005). The absolute pressure gauge is a Paroscientific depth sensor (model 8CB-4000) with a sampling interval of 15 s, which supplies static measurements with the 1 Pa (10^{-4} dbar) resolution necessary for tsunami detection. Pressure is also measured by a digital hydrophone (model SMID DT405D) with a sampling rate of 2 kHz, a resolution of 10^{-2} Pa, and a passband from 50 mHz to 1 kHz.

NON-EARTHQUAKE DATA AS EVIDENCE OF IONIAN SEAFLOOR INSTABILITY

The NEMO-SN1 seismometer worked well, recording different types of seismic signals, most of them local earthquakes, while also recording non-earthquake signals (Figure 2). The first type of signal not associated with fracturing processes is generated by a submarine landslide (Figure 2A). The second type

is a background seismic signal that exhibits harmonic behavior and has features strongly resembling those of volcanic tremor (Figure 2B). The third type of signal results from very short impulsive events (SDEs) that last about one second and show some peculiar properties (Figure 2C).

Efficient detection of seismic waves and accurate recognition of seismic phases from all distances is limited by the level of background noise in the frequency band of the signal. The main global sources of seismic noise are ocean waves (Webb, 1998). Attenuation of these waves along their pathways determines the noise level at a particular site. From past analyses, we estimated the broadband seismic noise at the NEMO-SN1 seafloor (Monna et al., 2014) and found that sea currents affect the seismic signal on all components below 0.1 Hz (Monna et al., 2005) and identified particular features of the seismic spectrum that depend on seasonal variations of the local climate (De Caro et al., in press).

SUBMARINE LANDSLIDES

Submarine landslide signals have high frequency content, lack easily recognizable P- and S-phases, and have longer durations than earthquake signals (Figures 2A and 3A). We summarize the results from Sgroi et al. (2007), who

analyzed landslide signals recorded by NEMO-SN1 during a stand-alone temporary deployment that captured the 2002–2003 Mt. Etna eruption.

In general, the seismic wavefield is composed of different waves (e.g., P- and S-body waves and surface waves) that move the ground in different directions. Polarization analysis helps us reconstruct the ground motion caused by the arrival of these different waves by measuring parameters (e.g., rectilinearity, incidence angles, azimuth) that characterize the types of motion. A low value of rectilinearity ($R \sim 0.6$) and incidence angles close to the horizontal plane ($> 80^\circ$) in our signals, values that are typical of surface waves, indicate planar wavefield composition (Figure 3A). The absence of body waves (P and S), the emerging onset of the signals, and their duration (ranging from tens of seconds to few minutes), lead us to conclude that these signals are definitely not a result of shear failure (typical of earthquakes). Their elliptical anticlockwise motion and incidence angles close to the horizontal plane suggest that the signals consist mainly of Rayleigh surface waves and have their source area within the seafloor at shallow depths. The epicentral distances of the events could not be estimated by the NEMO-SN1 observatory due to the absence of S-waves.

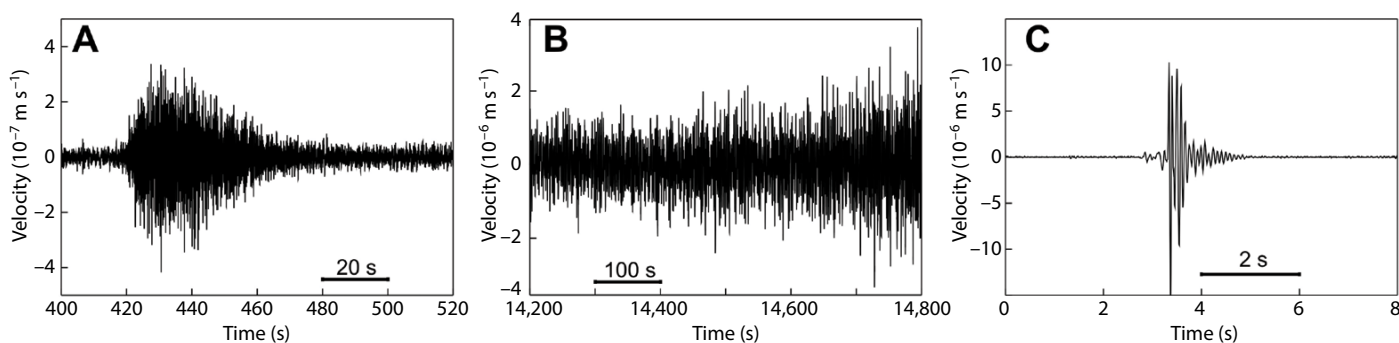


Figure 2. Example of waveforms (seismometer vertical component) of the three different types of signals analyzed in this study: (A) landslide; (B) volcanic tremor recorded during the onset of a lava fountain episode (the first episode occurred on February 19, 2013); (C) short duration event (SDE).

Given their characteristics, these signals were interpreted as submarine landslides (Sgroi et al., 2007). A rose diagram of the back-azimuth values of the events, centered at NEMO-SN1, can help identify the areas of major instability. Figure 3B shows the two main clusters: (1) 70°–110° (10 events), and (2) 240°–290° (10 events). It is also worth noting that a few of these landslides are preceded by a local or a regional earthquake, but a sound statistical analysis on a longer time series is needed to confirm this association. Oceanographic expeditions in the Ionian Sea confirmed the presence of deposits associated with submarine landslides.

The next step is to try to associate the areas identified in the rose diagram with the tectonic structures known from geological studies. The cluster between

240° and 290° may be associated with the Malta Escarpment, confirmed by the presence in the area of slumps consisting of unconsolidated sediments from the upper slope, which suggest the presence of a zone of active faulting at the base of the upper scarp (Adam et al., 2000). The other cluster, between 70° and 110°, could be associated with the “Messina Rise,” a large area of continental margin situated in southern Calabria and eastern Sicily crossed by the Messina canyon and submarine valleys (Sartori et al., 1991; Marani et al., 2004). This area is affected by diffuse mass-flow phenomena (slides and slumps) that have been identified in different stratigraphic levels by drilling. The maximum peak in the rose diagram (seven events in the 100°–110° sector; Figure 3B) might be related to instabilities in the

deep Ionian Basin, but supporting evidence (seismic, geological, bathymetric) is needed for this sector.

VOLCANIC TREMOR

Volcanic tremor is a continuous low-frequency seismic signal typically found in volcanic areas and usually associated with the underground movement of magma, fluids, or gases (Chouet, 1996). Although the eruption dynamics of Mt. Etna is well known, based on land data exclusively, the spatial extent and the shape of the plumbing system remain poorly understood. In fact, knowledge of the inner structure and magma storage zones is mostly limited to the part of the volcanic edifice above sea level, similar to Stromboli (Chouet et al., 2003).

In general, low-frequency seismic signals recorded on active volcanoes, such as tremor (Figure 2B) and long-period events, are interpreted as direct consequences of underground magmatic activity. Before and during an eruption, gas pockets rise within the magma column and interact with the conduit walls. This process causes vibration that produces a tremor signal whose energy is proportional to the volume and depth of the rising gas. This vibration precedes the explosive eruption by several seconds (e.g., Alparone et al., 2003).

In recent years, ocean bottom seismometers (OBSs) and seafloor observatories have frequently been used to monitor offshore seismic signals of volcanic origin (e.g., Butler et al., 2000; Caplan-Auerbach et al., 2001; Goslin et al., 2005; Sgroi et al., 2009). OBSs deployed on the East Pacific Rise have recorded micro-earthquakes associated with a mid-ocean ridge eruption (Tolstoy et al., 2006). Several studies based on pressure and seismic data recorded at the seafloor have focused on Axial Seamount

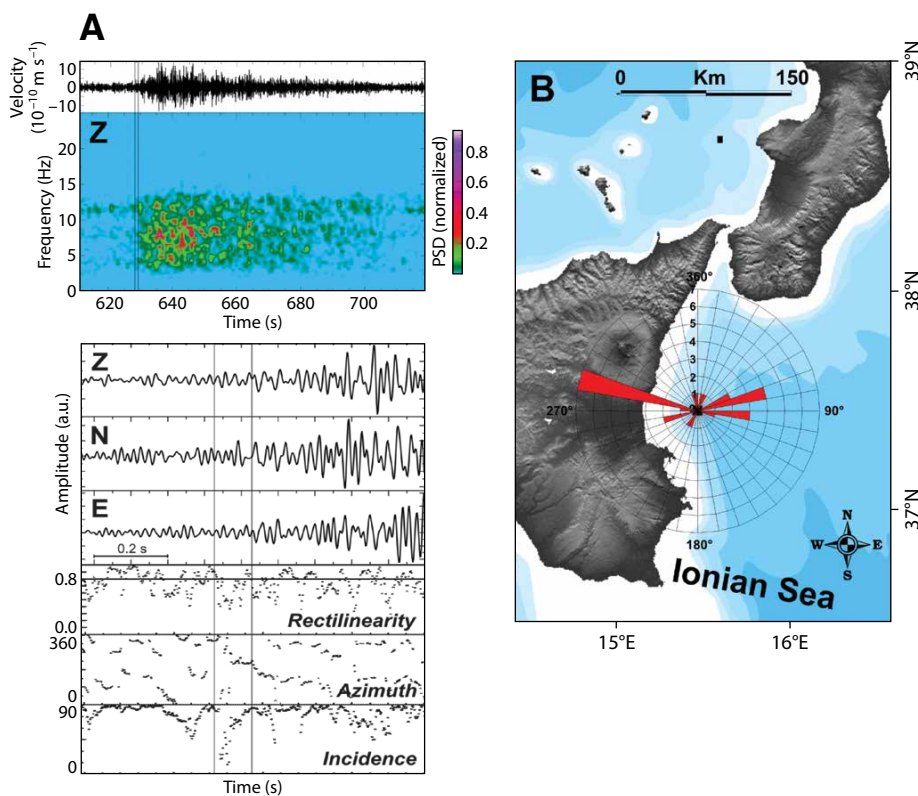


Figure 3. Submarine landslide signal: (A) waveform recorded by seismometer vertical component, corresponding spectrogram, and details of signal onset on the three components and polarization analysis in terms of rectilinearity, azimuth, and incidence angles (the gray lines define the time interval in which the polarization parameters are calculated). (B) Azimuthal distribution of submarine landslides. Modified from Monna et al. (2014)

on the Juan de Fuca Ridge (Fox et al., 2001). These studies show that the rate of seismicity (Dziak et al., 2012) and cycles of deflation and inflation (Chadwick et al., 2012), both caused by magma intrusion, can act as precursors to eruption onset. In this case, pressure variations measured at the ridge were caused by rising and lowering of the seafloor, which was in turn caused by magma intrusion and not by water above the pressure recorder.

Volcanic tremor plays a significant role in real-time volcano monitoring, as the pattern of this signal strongly reflects the evolution of the eruptive activity (Alparone et al., 2003). Continuous measurements of volcanic tremor (Figure 2B) can greatly enhance our comprehension of eruption mechanisms that produce considerable variations in chemical and physical properties of the volcanic edifice.

To detect the effects of volcanic activity on the seismic signals, we reconstructed the background seismic noise pattern recorded at the seafloor observatory (Figure 4C). The time series extends from September 2012 to May 2013.

Volcanic and nonvolcanic tremor in this area can be distinguished by the content of radiated energy within different frequency bands (Sgroi et al., 2013). They are the expression of two different mechanisms: volcanic tremor associated with volcanic activity, or nonvolcanic tremor linked to the stress induced by oceanographic parameters. To identify the contribution to background seismic noise of hydrostatic pressure variation on the seafloor from the overlying water column, seismometer data were compared with those recorded by the pressure gauge (Figure 4). Comparison between Figure 4B (pressure signal standard deviation, STD, computed

for a five-minute sliding window) and Figure 4C (seismic signal root mean square, RMS, computed for a one-minute window) shows that some of the peaks of the pressure signal are also visible in the seismic signal, so we interpret this energy as due to the

effect of the water column. The different effects on the seismic signal that result from a longer wavelength component caused by water column variations and microseismic noise are evident by comparing the pressure gauge (Figure 5C), hydrophone (Figure 5D), and 0.1–6 Hz

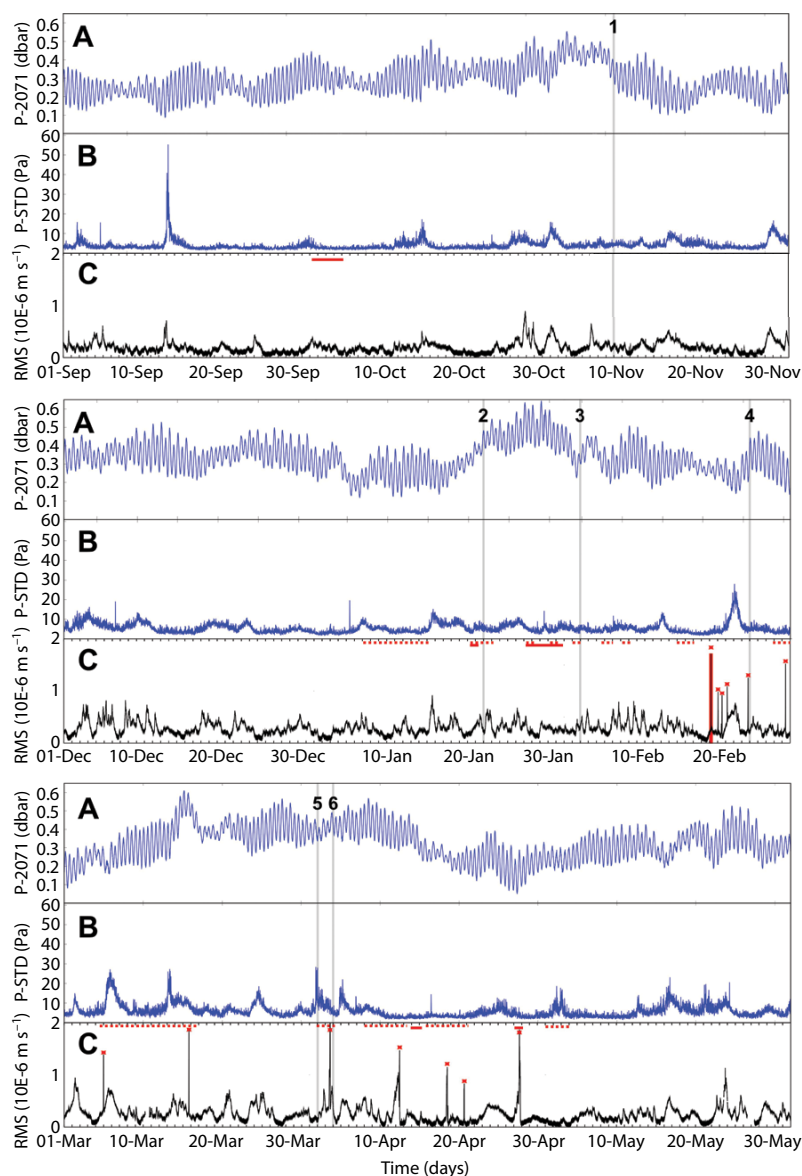


Figure 4. Continuous data for the nine months from September 2012 to May 2013. (A) Pressure (absolute pressure gauge). (B) Pressure standard deviation computed on a five-minute moving window. (C) RMS amplitude of seismic signal (vertical component of seismometer). The plot shows symbols (see legend) referring to three types of volcanic activity that occurred during the period analyzed. The gray vertical bars and the numbers identify periods of change in the slope of cumulative SDE energy (see Figure 5). The red rectangle marks the lava fountain episode shown in Figure 6.

bandpass filtered background noise (Figure 5E) signals. We conclude that the observed water pressure variations do not come from deformation of the seafloor in the NEMO-SN1 area caused by rising Etna magma. In fact, peak ground deformation measured on land is at most 25 cm (e.g., Bonaccorso, 1996), much smaller than deformation recorded on Axial Seamount (> 5 m) during the April 2011 eruption (Chadwick et al., 2012). Furthermore, our observation point is quite far from the area where the greatest ground deformation is measured.

We filtered out oceanic effects (the part related to nonvolcanic tremor) and found a correlation between the increase in volcanic tremor and

Mt. Etna activity, especially during lava fountain episodes. Thus, we focused on amplitude variations in the seismic signal produced by 13 lava fountain episodes that occurred between February 19 and April 27, 2013, and that were not observed in the absence of lava fountain episodes. Tremor variations recorded at NEMO-SN1 and at several stations on land show systematic relationships between rising magma, the beginning of the eruptive episode recorded at the surface, and an increase in tremor amplitude. Figure 6 compares tremor amplitudes recorded by seismometers on land and the NEMO-SN1 for the February 19 lava fountain episode (see location of stations in Figure 1). The spectrogram for data recorded by NEMO-SN1

(bottom of Figure 6) shows that tremor energy is concentrated between 0.5 Hz and 2 Hz, which is typical of a volcanic environment. As expected, maximum tremor amplitudes were recorded by the summit seismic station (designated ESLN), but, surprisingly, the next station with higher recorded amplitudes was NEMO-SN1 (Figure 6) at 2,100 m water depth and about 40 km ESE of the summit. Other land stations that detected a much smaller amplitude signal are at comparable distances from the summit as NEMO-SN1 (see Figure 1). Given this observation, it is likely that this signal is generated at the roots of the feeding system, which are located in the offshore ESE sector of the volcano. The location of Etna's roots has been identified by multichannel reflection profiles (e.g., Hirn et al., 1997), tomographic studies (e.g., Villaseñor et al., 1998), and GPS data (e.g., Bonforte and Puglisi, 2006). These studies suggest that tectonic structures located in eastern Sicily/Ionian Sea are preferential pathways for Mt. Etna's rising magma. This location agrees with observed gravitational instability of Mt. Etna's eastern-southern sector. In fact, Allard et al. (2006) proposed a link between magma accumulation below the volcano, flank instability, and the shift from continuous summit activity to episodic flank eruptions. They hypothesized the existence of areas of magma storage, placed at a depth of 3–5 km below sea level, that exert pressure on the eastern flank of the volcano, causing detachment and slippage of this portion of the volcanic edifice. We hypothesize a link between these magma storage areas, which extend under the seafloor, and the central feeding system of the volcano through which magma rises to reach the surface at the summit craters and cause lava fountaining.

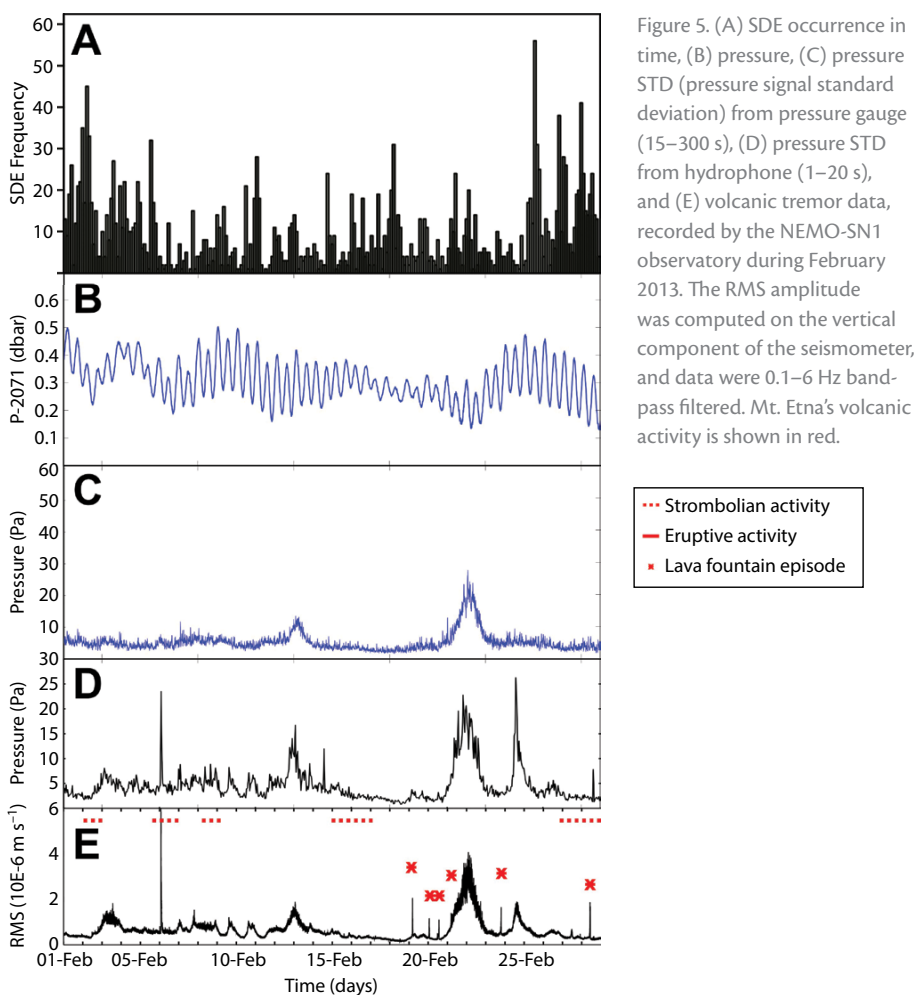


Figure 5. (A) SDE occurrence in time, (B) pressure, (C) pressure STD (pressure signal standard deviation) from pressure gauge (15–300 s), (D) pressure STD from hydrophone (1–20 s), and (E) volcanic tremor data, recorded by the NEMO-SN1 observatory during February 2013. The RMS amplitude was computed on the vertical component of the seismometer, and data were 0.1–6 Hz band-pass filtered. Mt. Etna's volcanic activity is shown in red.

SHORT DURATION EVENTS

Our data set includes a large number of short, impulsive signals that we generically call SDEs (Figures 2C and 7), in agreement with previous studies (e.g., Diaz et al., 2007). SDE swarms have been observed at the seafloor in hydrothermal and volcanic systems (e.g., Sohn et al., 1995). The main SDE features observed by the NEMO-SN1 seismometer are: (1) sharp, (2) high-frequency content (from about 10 Hz up to 50 Hz, the seismometer Nyquist frequency), (3) very short duration (about 1 s), and (4) very regular decrease of amplitude in the signal coda (Figure 2C). Inspection of the SDE data set revealed that most of these signals could be grouped into three families or clusters on the basis of their waveform and frequency content (Figure 7). The first family (Figure 7A) includes events exhibiting a monochromatic spectrum with a dominant spectral peak either of low frequency (about 12 Hz) or high frequency (about 25 Hz). The second family (Figure 7B) includes events that have a bimodal spectrum with two main peaks, one in the low-frequency and the other in the high-frequency range. The third family (Figure 7C) consists of events characterized by rich and complex spectra with energy from 10 Hz to 50 Hz.

In total, about 23,000 SDEs were recorded in nine months. The number of SDEs per day varied between nine and 350, with a median value of 73 events per day. In general, SDE amplitudes vary from about 0.1 mm s^{-1} (just above ambient noise) to tens of mm s^{-1} . Particle motion analysis of a subset of 53 SDEs shows that there is a preferential (90% of the total) NNE–SSW direction ($\sim 15^\circ$) and, for a smaller number (10%), the direction is roughly E–W ($\sim 300^\circ$). In some cases, the first wavelet

can be identified as a body wave from its linear three-dimensional motion (Figure 7B); in other cases, we observe the typical nonlinear motion of surface waves (Figure 7A,C). The signals of the most energetic SDEs are also visible in the pressure data (hydrophone, Figure 7D,E), which shows perfect agreement in detection time for the two sensors. The frequency analysis reveals rich energy content, also at higher frequency (40–80 Hz, Figure 7D,E), superimposed on a very noisy background signal. Difficulties in identifying the less-energetic SDEs on the hydrophone are likely caused by the high noise level (or signals from other sources) in the frequency band of interest (10–30 Hz), and by the fact that shear energy does

not propagate in water. Detection of SDE high-frequency energy (which rapidly attenuates as the wave travels) by the hydrophone between 40 Hz and 75 Hz (well beyond the seismometer Nyquist at 50 Hz) points to the small scale of the SDE generation process and to a nearby source. As we only have data from one seismic station, we cannot accurately locate the SDE source. The proximity of the SDEs to the observatory is confirmed by the fact that the dense on-land network does not detect them. Furthermore, the particle motion is mostly in the near-horizontal direction, implying that the source is shallow.

Previous studies in other areas estimated a distance of the SDE source from the sensor to be on the order

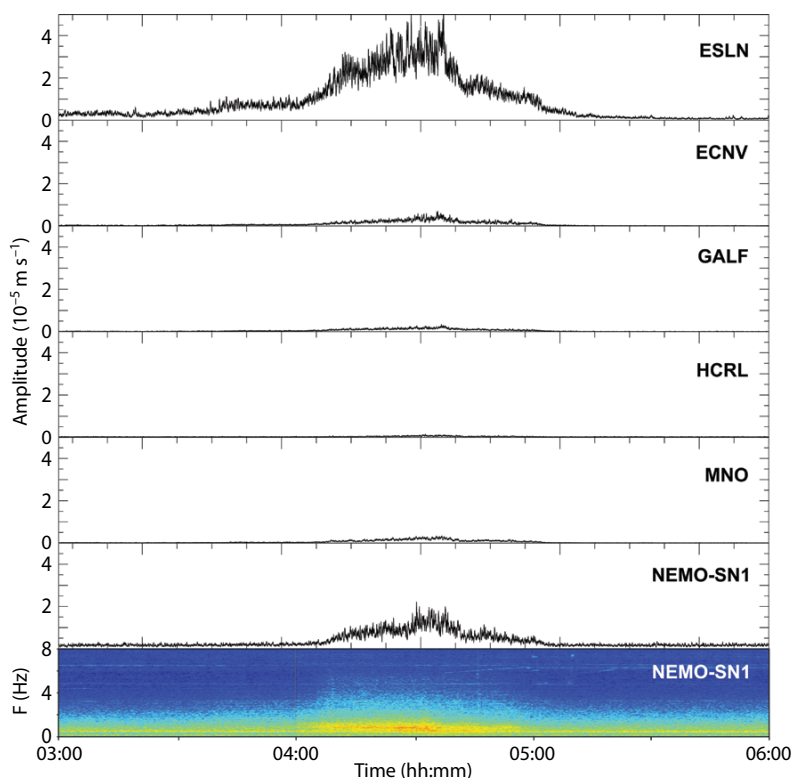


Figure 6. Comparison of tremor data recorded by land stations and NEMO-SN1 during the lava fountain episode of February 19, 2013. Summit station ESLN recorded the maximum amplitude during this episode. Surprisingly, the NEMO-SN1 seafloor observatory recorded the second highest value in tremor amplitude. A NEMO-SN1 spectrogram at the bottom of the figure shows that energy during the lava fountain is concentrated in the band 0.5–2 Hz (warm colors indicate frequencies with higher energy content).

of hundreds of meters (Sultan et al., 2011) or even tens of meters (Tary et al., 2012). SDE generation has been associated with a number of possible sources, including fluid-filled cracks in sedimentary basins (Diaz et al., 2007) and gas seepage (Tary et al., 2012; Embriaco et al., 2014). Another possible source of SDEs is of biological origin (Buskirk et al., 1981; Bowman and Wilcock, 2014). Because there are not a large number of organisms living at 2,100 m depth, we conclude it is unlikely that fish or other organisms hitting the sensors are sources of the large number of SDEs, as confirmed by film footage

taken near the seafloor. Furthermore, because the seismometer is protected by the observatory's metal frame and also by a metal bell that covers the sensor vessel, we would expect a more ringing and monochromatic signal if organisms hitting these metal parts were the source of the SDEs. Also, contrary to Bowman and Wilcock (2014), we find preferential directions in the particle motion of a subset of analyzed SDEs (mostly E-W and also NNE-SSW; Figure 7A–C), and we do not find a diurnal distribution of SDE events.

Sohn et al. (1995) modeled complex SDE waveforms based on hydraulic

fracturing within a seafloor hydrothermal system. Using similar modeling, Diaz et al. (2007) explained the SDEs as pressure transients generated by fluid-filled cracks. A vibrating fluid model predicts well-defined peaks, while a model based on a small fracture is in agreement with a broader band spectrum. In fact, the SDE waveforms are similar to the waveforms recorded in hydrofracturing experiments (Sohn et al., 1995, and references therein). On the basis of this information, we propose that hydraulic fracturing of rocks is the most likely source of the SDEs that we detected. Given their shallow depth

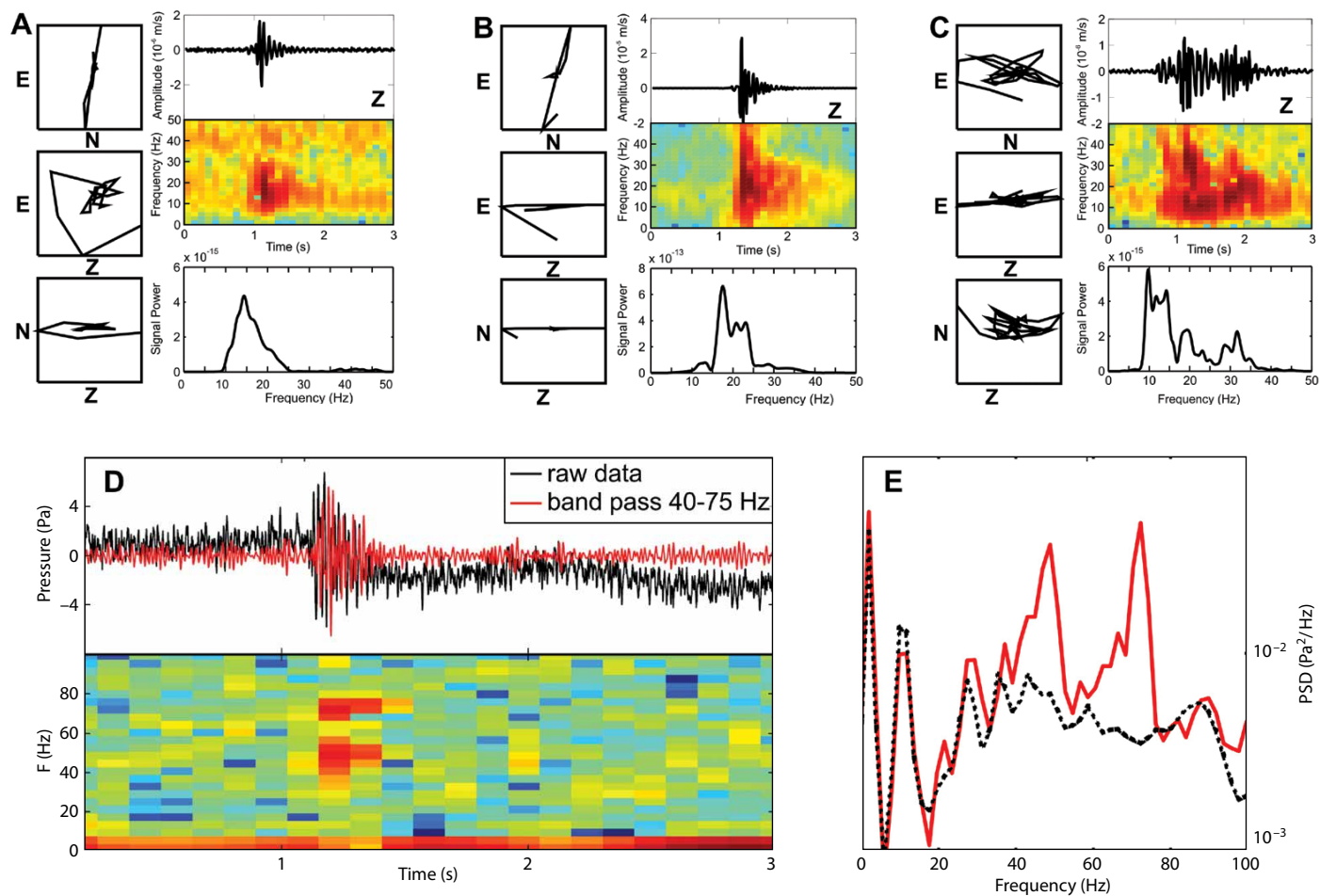


Figure 7. Examples of SDE signals in time and frequency domains. Boxes A to C include particle motion, vertical component waveform, spectrogram, and spectrum for the three different SDE families: (A) monochromatic, (B) bimodal, and (C) complex. (D) An example of energetic SDE recorded by the hydrophone (black curve, unfiltered data; red curve, filtered data) with spectrogram. (E) The power spectral density (PSD) of the same SDE. An STA/LTA (short time average/long time average) algorithm was applied to the continuous seismic waveform to automatically detect SDEs. The trace was high-pass Butterworth filtered with a corner frequency of 8 Hz and four poles. We estimated that about 8% are false triggers with low energy.

and their particle motion, the likely candidates for SDE generation are the fluid-filled carbonate outcrops found at the base of the Malta Escarpment (Argnani and Bonazzi, 2005), where NEMO-SN1 was deployed. Because SDEs are generated continuously, the hydraulic fracturing must be occurring continuously.

We investigated a possible correlation between the time distribution of SDEs, Mt. Etna lava fountain episodes, and pressure variations (Figure 5). A correlation between seismic energy release and water column pressure tidal variation was observed at the seafloor at Axial Seamount (Tolstoy et al., 2002). Wilcock (2001) demonstrated tidal triggering of ridge-parallel micro-earthquakes from normal faults. Our observations show that there is no apparent correlation between SDE occurrence and water tidal variations (Figure 5), suggesting that the changes in hydrostatic pressure are not responsible for SDE generation, or at least are not a main driving mechanism.

To investigate possible correlation between SDE generation and sea pressure, we performed various statistical tests. We verified that in the power spectral density of SDE occurrences in time, no significant peaks correspond to the principal tidal constituents (diurnal, semidiurnal). Longer periodicity (~ 5 days) has been observed in the SDE series (Figure 5A,B), but they are not consistently observed in the whole time series. Furthermore, we compute the correlation between pressure values and SDE occurrence in time, revealing negligible linear correlation (correlation coefficient = 0.003). Similar results are found for the correlation between the SDE first and second pressure derivatives. A reasonable explanation is that tidal variations in water-column pressure

in the Ionian Sea are too small (on the order of 0.1 dbars). In fact, they are an order of magnitude smaller than the variations observed by Wilcock (2001) and Tolstoy et al. (2002) in the Pacific Ocean. Thus, we may conclude that at this site, no correlation exists between SDE occurrence and pressure loading changes (including tidal and no tidal variation); instead, we should consider an association between SDE generation and Mt. Etna activity.

Figure 8 shows a plot of the cumulative sum of the SDE energy over nine months (red curve). The SDE energy is measured as the maximum of the average of the signal squared amplitude on a 2 s moving window. If we compare the observed cumulative sum energy

to a set of 1,000 randomly generated energy cumulative sums (black curves in Figure 8), we see that the observed curve behaves quite differently from the pattern of the random cumulative sums. This difference is confirmed by comparing the median (blue) curve with the 0.01 and 0.99 percentile (green) curves (analysis performed using the software R; R Core Team, 2012). This analysis shows that the accumulated SDE energy is the result of some driving mechanism and not of a random process. We can divide the observation period into two parts by comparing the slope of the observed cumulative sum (red curve) and of the median cumulative sum (blue curve) of the random processes: the first part up to point 2, and the second

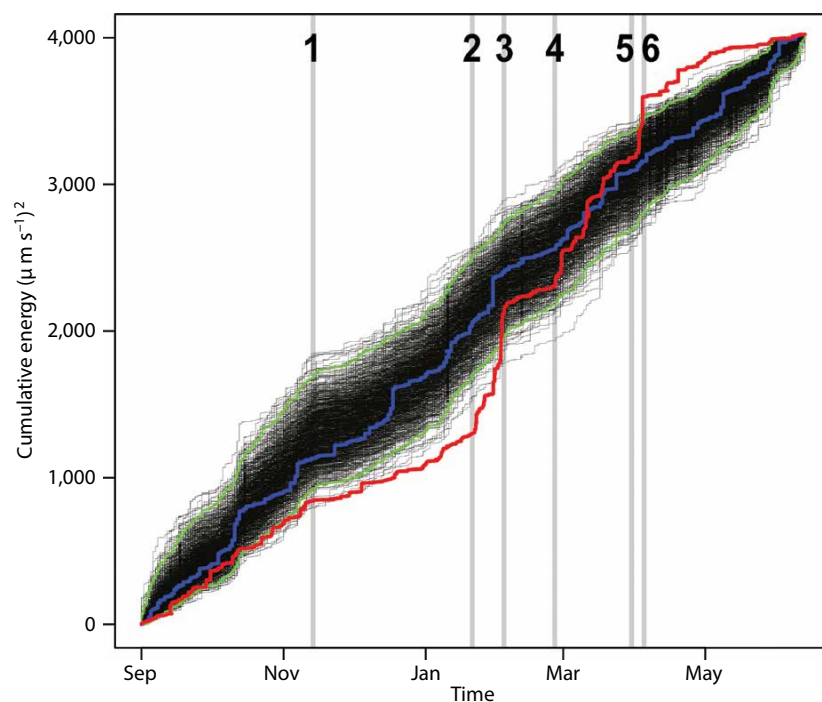


Figure 8. Cumulative energy curve for SDEs during September 2012 to May 2013 (red curve), cumulative energy curves from 1,000 random processes (black curves), median cumulative energy (blue curve), and 0.01 and 0.99 percentile curves (green curves). Each simulated process is made up of 23,000 SDEs, and the processes are produced by transforming the energy values of each SDE in the various times of occurrence (which remain fixed). Vertical gray lines and numbers identify periods in which there is a change in the slope of the energy aggregate. The times at which these changes occur are also reported in Figure 4 to compare changes in the SDE generation process with the tremor pattern and volcanic activity.

part between points 2 and 6. The slope represents the rate at which energy is accumulated; in the first part, the rate of SDE energy release is small compared to the median rate (especially from point 1 to 2), while most of the SDE energy release is in the second period. The time intervals (numbers in Figure 8) in which there is a change in speed of SDE energy release can be compared with Mt. Etna activity as measured by the root mean square (RMS; Figure 4). Referring to Figure 4, we see that interval from 1–2 is a period of scarce explosive activity, while intervals 2–6 correspond to a period in which Mt. Etna is very active and the seismometer recorded signals linked to lava fountain episodes. If the Mt. Etna/SDE association is valid, then

lead to a change in the fracturing regime. As we have seen for the lava fountains, signals generated by Mt. Etna dynamics are recorded clearly at NEMO-SN1, so it is not surprising that the SDE generation process is sensitive to Mt. Etna activity.

CONCLUSIONS

The instability of the Western Ionian seafloor is linked to Mt. Etna volcanism and to tectonic structures that are potential sources of destructive earthquakes. A multidisciplinary approach with NEMO-SN1 helps to identify the driving mechanism for non-earthquake signals. Submarine landslides and some of their possible source locations have been inferred from the NEMO-SN1 seismometer. Most of these events

affected by diffuse mass-flow phenomena such as slides and slumps.

Tremor amplitude increases at the same time as explosive volcanic activity. The seismic stations that are closer to the summit craters, where the explosive activity occurs, consequently record higher tremor amplitudes. Surprisingly, these phenomena were clearly observed at 2,100 m water depth at about 40 km from Mt. Etna's summit during a cycle of lava fountaining from February to April 2013. This means that lava fountains are in fact generated by processes deep and energetic enough to produce seismic waves that are more efficiently detected at NEMO-SN1 than at land stations located at similar distances from the summit area (excluding the summit ESLN station, the closest). The fact that tremor associated with lava fountain episodes is clearly detected by NEMO-SN1 supports the hypothesis of an offshore location for the roots of the Mt. Etna feeding system.

The other interesting phenomenon observed at NEMO-SN1 is the continuous occurrence of high-frequency, impulsive SDEs. We explain the continuous SDE generation as hydrofracturing of nearby fluid-filled carbonate outcrops. In certain time intervals, SDE generation cannot be described as a random process, and the most likely candidate for a driving mechanism is Mt. Etna dynamics. Changes in the slope of the SDE energy cumulative sum could be associated with Mt. Etna's rest and active periods. Active phases are associated with increased tremors resulting from lava fountain episodes, which are detected by NEMO-SN1. More data need to be analyzed to achieve greater statistical significance, but this can be considered a first step in finding a correlation between SDEs recorded at

“ THE INSTABILITY OF THE WESTERN IONIAN SEAFLOOR IS LINKED TO MT. ETNA VOLCANISM AND TO TECTONIC STRUCTURES THAT ARE POTENTIAL SOURCES OF DESTRUCTIVE EARTHQUAKES. ”

interval 1–2 represents a “rest” phase that is preparatory to the “active” 2–6 phase.


What could be the link between Mt. Etna's activity and the generation of SDEs? We propose the following hypothesis: Mt. Etna in its active stages (before and during an eruption) changes the stress field in the surrounding area, causing decreased or increased hydrofracturing of carbonate rocks, and thus a change in detected SDE energy. As the fluid-filled rock is always ready to crack (continuously generating SDEs), even small changes in the stress field can

were preceded by local and regional earthquakes, so a link between the occurrence of submarine landslides and tectonic structures that lie in the area can be inferred. This association may be confirmed using a rose diagram of submarine landslide distribution. It shows two main tectonic structures that could be responsible for landslide occurrence. The main cluster can be associated with the tectonic structure of the Malta Escarpment, while the secondary cluster can be associated with the “Messina Rise,” a large area of continental margin

the Western Ionian seafloor and Mt. Etna activity. This analysis is promising and offers an interesting insight into a complex chain of events.

While lava fountain episodes and SDE signals can be associated with gas movement caused by Mt. Etna volcanism, submarine landslides originate from tectonic movement. Given the likely location of Mt. Etna roots, there is a complex interplay between tectonics and volcanism. Because NEMO-SN1 is now a permanent node of the Italian Seismic Network, we plan to analyze more data during other eruptive episodes in order to incorporate the additional statistics needed to confirm that the SDE generation process might act as a “sensor” for Mt. Etna activity, and to investigate a possible precursory role for the SDE signals.

ACKNOWLEDGMENTS

We thank the editor Ellen Kappel for her courteous encouragement, and reviewers Robert P. Dziak, William S.D. Wilcock, and Martin Heesemann, who provided very helpful comments and detailed notes that improved this article. We thank D.-T. Ton-That for useful suggestions on the text. 

REFERENCES

- Adam, J., C.D. Reuther, M. Grasso, and L. Torelli. 2000. Active fault kinematics and crustal stresses along the Ionian margin of southeastern Sicily. *Tectonophysics* 326:217–239, [http://dx.doi.org/10.1016/S0040-1951\(00\)00141-4](http://dx.doi.org/10.1016/S0040-1951(00)00141-4).
- Allard, P., B. Behncke, S. D’Amico, M. Neri, and S. Gambino. 2006. Mount Etna 1993–2005: Anatomy of an evolving eruptive cycle. *Earth-Science Reviews* 78:85–114, <http://dx.doi.org/10.1016/j.earscirev.2006.04.002>.
- Alparone, S., D. Andronico, L. Lodato, and T. Sgroi. 2003. Relationship between tremor and volcanic activity during the Southeast Crater eruption on Mount Etna in early 2000. *Journal of Geophysical Research* 108, 2241, <http://dx.doi.org/10.1029/2002JB001866>.
- Argnani, A. 2009. Evolution of the southern Tyrrhenian slab tear and active tectonics along the western edge of the Tyrrhenian subducted slab. *Geological Society Special Publication* 311:193–212, <http://dx.doi.org/10.1144/SP311.7>.
- Argnani, A., and C. Bonazzi. 2005. Malta Escarpment fault zone offshore eastern Sicily: Pliocene-Quaternary tectonic evolution based on new multichannel seismic data. *Tectonics* 24, TC4009, <http://dx.doi.org/10.1029/2004TC001656>.
- Ben-Avraham, Z., V. Lyakhovsky, and M. Grasso. 1995. Simulation of collision zone segmentation in the central Mediterranean. *Tectonophysics* 243:57–68, [http://dx.doi.org/10.1016/0040-1951\(94\)00191-B](http://dx.doi.org/10.1016/0040-1951(94)00191-B).
- Bianca, M., C. Monaco, L. Tortorici, and L. Cernobori. 1999. Quaternary normal faulting in south-eastern Sicily (Italy): A seismic source for the 1693 large earthquake. *Geophysical Journal International* 139:370–394, <http://dx.doi.org/10.1046/j.1365-246x.1999.00942.x>.
- Bonaccorso, A. 1996. Dynamic inversion of ground deformation data for modeling volcanic sources (1991–93). *Geophysical Research Letters* 23:451–454, <http://dx.doi.org/10.1029/96GL00418>.
- Bonforte, A., and G. Puglisi. 2006. Dynamics of the eastern flank of Mt. Etna volcano (Italy) investigated by a dense GPS network. *Journal of Volcanology and Geothermal Research* 153:357–369, <http://dx.doi.org/10.1016/j.jvolgeores.2005.12.005>.
- Borgia, A., P.T. Delaney, and P. Denlinger. 2000. Spreading volcanoes. *Annual Review of Earth and Planetary Sciences* 28:539–570, <http://dx.doi.org/10.1146/annurev.earth.28.1.539>.
- Borgia, A., L. Ferrari, and G. Pasquarè. 1992. Importance of gravitational spreading in the tectonic and volcanic evolution of Mount Etna. *Nature* 37:231–235, <http://dx.doi.org/10.1038/357231a0>.
- Boschi, E., E. Guidoboni, G. Ferrari, D. Mariotti, G. Valensise, and P. Gasperini. 2000. Catalogue of strong Italian earthquakes from 461 BC to 1997. *Annals of Geophysics*, appendix to 43(4):609–868 (with database on CD-ROM).
- Bowman, D.C., and W.S.D. Wilcock. 2014. Unusual signals recorded by ocean bottom seismometers on the caldera floor of Deception Island volcano, Antarctica. *Antarctic Science* 26:267–275, <http://dx.doi.org/10.1017/S0954102013000758>.
- Branca, S., M. Coltelli, and G. Groppe. 2011. Geological evolution of a complex basaltic stratovolcano: Mount Etna, Italy. *Italian Journal of Geoscience* 130:306–317, <http://dx.doi.org/10.3301/IJG.2011.13>.
- Buskirk, R.E., C. Frohlich, G.V. Latham, A.T. Chen, and J. Lawton. 1981. Evidence that biological activity affects ocean bottom seismograph recordings. *Marine Geophysical Researches* 5:189–205.
- Butler, R., A.D. Chave, F.K. Duennebie, D.R. Yoeberger, R. Pettit, D. Harris, F.B. Wooding, A.D. Bowen, J. Bailey, J. Jolly, and others. 2000. Hawaii-2 observatory pioneers opportunities for remote instrumentation in ocean studies. *Eos Transactions, American Geophysical Union* 81(15):157–163, <http://dx.doi.org/10.1029/00EO00105>.
- Caplan-Auerbach, J., C.G. Fox, and F.K. Duennebie. 2001. Hydroacoustic detection of submarine landslides on Kilauea volcano. *Geophysical Research Letters* 28:1,811–1,813, <http://dx.doi.org/10.1029/2000GL012545>.
- Chadwick, W.W. Jr., S.L. Nooner, D.A. Butterfield, and M.D. Lilley. 2012. Seafloor deformation and forecasts of the April 2011 eruption at Axial Seamount. *Nature Geoscience* 5:474–477, <http://dx.doi.org/10.1038/ngeo1464>.
- Chierici, F., P. Favali, L. Beranzoli, A. De Santis, D. Embriaco, G. Giovanetti, G. Marinaro, S. Monna, L. Pignagnoli, G. Riccobene, F. Bruni, and F. Gasparoni. 2012. NEMO-SN1 (Western Ionian Sea, off Eastern Sicily): A cabled abyssal observatory with tsunami early warning capability. Pp. 130–137 in *Proceedings of the 22nd (2012) International Offshore and Polar Engineering Conference*, Rhodes, Greece, June 17–22, 2012.
- Chouet, B. 1996. Long-period volcano seismicity: Its source and use in eruption forecasting. *Nature* 380:309–316, <http://dx.doi.org/10.1038/380309a0>.
- Chouet, B., P. Dawson, T. Ohminato, M. Martini, G. Saccorotti, F. Giudicepietro, G. De Luca, G. Milana, and R. Scarpa. 2003. Source mechanisms of explosions at Stromboli Volcano, Italy, determined from moment-tensor inversions of very-long-period data. *Journal of Geophysical Research* 108, 2019, <http://dx.doi.org/10.1029/2002JB001919>.
- Dalyander, P.S., B. Butman, C.R. Sherwood, R.P. Signell, and J.L. Wilkin. 2013. Characterizing wave- and current-induced bottom shear stress: US middle Atlantic continental shelf. *Continental Shelf Research* 52:73–86, <http://dx.doi.org/10.1016/j.csr.2012.10.012>.
- De Caro, M., S. Monna, F. Frugoni, L. Beranzoli, and P. Favali. In press. Seafloor seismic noise at Central-Eastern Mediterranean sites. *Seismological Research Letters*.
- Diaz, J., J. Gallart, and J. Gaspà. 2007. Atypical seismic signals at the Galicia Margin, North Atlantic Ocean, related to the resonance of subsurface fluid-filled cracks. *Tectonophysics* 433:1–13, <http://dx.doi.org/10.1016/j.tecto.2007.01.004>.
- Dziak, R.P., J.H. Haxel, D.R. Bohnenstiehl, W.W. Chadwick Jr., S.L. Nooner, M.J. Fowler, H. Matsumoto, and D.A. Butterfield. 2012. Seismic precursors and magma ascent before the April 2011 eruption at Axial Seamount. *Nature Geoscience* 5:478–482, <http://dx.doi.org/10.1038/ngeo1490>.
- Embriaco, D., G. Marinaro, F. Frugoni, S. Monna, G. Etiope, L. Gasperini, A. Polonia, F. Del Bianco, M.N. Çağatay, U.B. Ulgen,

- and P. Favali. 2014. Monitoring of gas and seismic energy release by multiparametric benthic observatory along the North Anatolian Fault in the Sea of Marmara (NW Turkey). *Geophysical Journal International* 196:850–866, <http://dx.doi.org/10.1093/gji/ggt436>.
- Favali, P., F. Chierici, G. Marinaro, G. Giovanetti, A. Azzarone, L. Beranzoli, A. De Santis, D. Embriaco, S. Monna, N. Lo Bue, and others. 2013. NEMO-SN1 abyssal cabled observatory in the Western Ionian Sea. *IEEE Journal of Oceanic Engineering* 38:358–374, <http://dx.doi.org/10.1109/JOE.2012.2224536>.
- Favali, P., R. Person, C.R. Barnes, Y. Kaneda, J.R. Delaney, and S.-K. Hsu. 2010. Seafloor observatory science. In *Proceedings of the OceanObs'09: Sustained Ocean Observations and Information for Society*. J. Hall, D.E. Harrison, and D. Stammer, eds, Venice, Italy, September 21–25, 2009, ESA Publication WPP-306, <http://www.oceanobs09.net/proceedings/cwp/Favali-OceanObs09.cwp.28.pdf>.
- Fox, C.G., W.W. Chadwick Jr., and R.W. Embley. 2001. Direct observation of a submarine volcanic eruption from a sea-floor instrument caught in a lava flow. *Nature* 412:727–729, <http://dx.doi.org/10.1038/35089066>.
- Goslin, J., N. Louren, R.P. Dziak, D.R. Bohnenstiehl, J. Haxel, and J. Luis. 2005. Long-term seismicity of the Reykjanes Ridge (North Atlantic) recorded by a regional hydrophone array. *Geophysical Journal International* 162:516–524, <http://dx.doi.org/10.1111/j.1365-246X.2005.02678.x>.
- Hirn, A., R. Nicolich, J. Gallart, M. Laigle, L. Cernobori, and ETNASEIS Scientific Group. 1997. Roots of Etna volcano in faults of great earthquakes. *Earth and Planetary Science Letters* 148:171–191, [http://dx.doi.org/10.1016/S0012-821X\(97\)00023-X](http://dx.doi.org/10.1016/S0012-821X(97)00023-X).
- Marani, M.P., F. Gamberi, G. Bortoluzzi, G. Carrara, M. Ligi, and D. Penitenti. 2004. Seafloor bathymetry of the Ionian Sea. Plate 3 in *From Seafloor to Deep Mantle: Architecture of the Tyrrhenian Backarc Basin*. M.P. Marani, F. Gamberi, and E. Bonatti, eds, *Memorie Descrittive Carta Geologica d'Italia*, vol. 44.
- McGuire, W.J. 1996. Volcano instability: A review of contemporary themes. Pp. 1–23 in *Volcano Instability on the Earth and other Planets*. W.J. McGuire, A.P. Jones, and J. Neuberg, eds, Geological Society Special Publication, vol. 110.
- Meletti, C., E. Patacca, and P. Scandone. 2000. Construction of a seismotectonic model: The case of Italy. *Pure and Applied Geophysics* 157:11–35, <http://dx.doi.org/10.1007/PL00001089>.
- Monna, S., G. Falcone, L. Beranzoli, F. Chierici, G. Cianchini, M. De Caro, A. De Santis, D. Embriaco, F. Frugoni, G. Marinaro, and others. 2014. Underwater geophysical monitoring for European Multidisciplinary Seafloor and water column Observatories. *Journal of Marine Systems* 130:12–30, <http://dx.doi.org/10.1016/j.jmarsys.2013.09.010>.
- Monna, S., F. Frugoni, C. Montuori, L. Beranzoli, and P. Favali. 2005. High quality seismological recordings from the SN1 deep seafloor observatory in the Mt. Etna region. *Geophysical Research Letters* 32, L07303, <http://dx.doi.org/10.1029/2004GL021975>.
- R Core Team. 2012. *R: A Language and Environment for Statistical Computing*. R Foundation for Statistical Computing, Vienna, Austria, <http://www.lsw.uni-heidelberg.de/users/christlieb/teaching/UKStaSS10/R-refman.pdf>.
- Sartori, R., M.L. Colalongo, G. Gabbianelli, C. Bonazzi, S. Carbone, P. Curzi, D. Evangelisti, M. Grasso, F. Lentini, S. Rossi, and L. Selli. 1991. Note stratigrafiche e tettoniche sul “Rise di Messina” (Ionio nord occidentale). *Giornale di Geologia* 53(2):49–64.
- Scandone, P., E. Patacca, R. Radoicic, W.B.F. Ryan, M.B. Cita, M. Rawson, H. Chezar, E. Miller, J. McKenzie, and S. Rossi. 1981. Mesozoic and Cenozoic rocks from the Malta Escarpment (central Mediterranean). *Bulletin of the American Association of Petroleum Geologists* 65:1,299–1,319.
- Sgroi, T., L. Beranzoli, G. Di Grazia, A. Ursino, and P. Favali. 2007. New observations of local seismicity by the SN1 seafloor observatory in the Ionian Sea, off-shore Eastern Sicily (Italy). *Geophysical Journal International* 169:490–501, <http://dx.doi.org/10.1111/j.1365-246X.2007.03348.x>.
- Sgroi, T., M. De Caro, N. Lo Bue, and P. Favali. 2013. Insights of the Mt. Etna volcanic activity through multiparametric data recorded by the NEMO-SN1 seafloor observatory. *Mineralogical Magazine* 77(5):2,184 (abstract), <http://goldschmidt.info/2013/abstracts/finalPDFs/2184.pdf>.
- Sgroi, T., C. Montuori, R. Agrusta, and P. Favali. 2009. Low-frequency seismic signals recorded by OBS at Stromboli volcano (Southern Tyrrhenian Sea). *Geophysical Research Letters* 36, L04305, <http://dx.doi.org/10.1029/2008GL036477>.
- Sohn, R.A., J.A. Hildebrand, S.C. Webb, and C.G. Fox. 1995. Hydrothermal microseismicity at the Megaplume site on the southern Juan de Fuca Ridge. *Bulletin of the Seismological Society of America* 85:775–778.
- Sultan, N., V. Riboulot, S. Ker, B. Marsset, L. Géli, J.B. Tary, F. Klingelhoefer, M. Voisset, V. Lanfumey, J.L. Colliat, and others. 2011. Dynamics of fault-fluid-hydrate system around a shale-cored anticline in deepwater Nigeria. *Journal of Geophysical Research* 116, B12110, <http://dx.doi.org/10.1029/2011JB008218>.
- Tary, J.B., L. Géli, C. Guennou, P. Henry, N. Sultan, M.N. Çağatay, and V. Vidal. 2012. Microevents produced by gas migration and expulsion at the seabed: A study based on sea bottom recordings from the Sea of Marmara. *Geophysical Journal International* 190:993–1,007, <http://dx.doi.org/10.1111/j.1365-246X.2012.05533.x>.
- Tinti, S., A. Maramai, and L. Graziani. 2004. The new catalogue of Italian tsunamis. *Natural Hazards* 33:439–465, <http://dx.doi.org/10.1023/B:NHAZ.0000048469.51059.65>.
- Tolstoy, M., E.T. Baker, D.J. Fornari, K.H. Rubin, T.M. Shank, F. Waldhauser, D.R. Bohnenstiehl, D.W. Forsyth, R.C. Holmes, B. Love, and others. 2006. A sea-floor spreading event captured by seismometers. *Science* 314:1,920–1,922, <http://dx.doi.org/10.1126/science.1133950>.
- Tolstoy, M., F.L. Vernon, J.A. Orcutt, and F.K. Wyatt. 2002. Breathing of the seafloor: Tidal correlations of seismicity at Axial volcano. *Geology* 30:503–506, [http://dx.doi.org/10.1130/0091-7613\(2002\)030<0503:BOTSTC>2.0.CO;2](http://dx.doi.org/10.1130/0091-7613(2002)030<0503:BOTSTC>2.0.CO;2).
- Villaseñor, A., H.M. Benz, L. Filippi, G. De Luca, R. Scarpa, G. Patanga, and S. Vinciguerra. 1998. Three-dimensional P-wave velocity structure of Mt. Etna, Italy. *Geophysical Research Letters* 25:1,975–1,978, <http://dx.doi.org/10.1029/98GL01240>.
- Webb, S.C. 1998. Broadband seismology and noise under the ocean. *Reviews of Geophysics* 36:105–142, <http://dx.doi.org/10.1029/97RG02287>.
- Wilcock, W.S.D. 2001. Tidal triggering of microearthquakes on the Juan de Fuca Ridge. *Geophysical Research Letters* 28:3,999–4,002, <http://dx.doi.org/10.1029/2001GL013370>.